Liquid film dewetting induced by impulsive Joule heating

H. C. Mayer
Department of Mechanical Engineering, University of California, Santa Barbara, California 93106, USA

R. Krechetnikov
Department of Mathematical and Statistical Sciences, University of Alberta, Edmonton, Alberta T6G 2G1, Canada

(Received 4 May 2017; published 15 September 2017)

Motivated by the need for understanding the boiling processes in three-phase microscopic systems, the present work aims to uncover the physics of forced dewetting of a liquid film initially attached to a metal wire frame, which is heated with a rate up to $O(10^8)\,\mathrm{K\,s^{-1}}$ by discharging a capacitor impulsively. Depending on the corresponding heat flux $\leqslant O(10^{11})\,\mathrm{J\,m^{-2}}$, there are several key dewetting regimes—no detachment, nonuniform detachment, and uniform detachment of a film—differentiated by boiling transitions in the film Plateau borders. Transitions between these regimes prove to occur, for various wire diameters and frame sizes, around the same values of the capacitor energy per unit wire volume. Also, an intrinsic transverse instability manifesting itself in the formation of fingers along the detached liquid film rim is discovered and analyzed in detail.

DOI: 10.1103/PhysRevFluids.2.094003

I. INTRODUCTION

Development of new technologies stimulates new fundamental questions: inkjet printing [1,2] is a good illustration of how explosive boiling of a liquid film was never thought to be useful until such a technology was invented. As we know today, it relies upon the formation (nucleation), growth, and subsequent collapse of a microscopic bubble of vaporized ink leading to droplet ejection. The behavior of ink under superheated conditions determines stability of this process. Among other modern heat-transfer problems are cooling of high-heat-flux miniature electronic devices, high pulsed heating, and vapor explosions on microheaters. The associated heating rates often exceed 10^7 K/s, so that the liquid quickly enters a highly superheated state with rapid boiling and evaporation occurring under strong nonequilibrium conditions.

The motivation for the present study is threefold. First, development of thermal micromachinery and microgenerators as well as miniaturization of electronics and high power and/or voltage devices [3] made the liquid phase used for cooling prone to superheated conditions. Second, while boiling is usually studied either in steady regime on flat [4] or curved [5] surfaces or in a fast transient regime also on flat or curved [2,6–8] surfaces, in all these studies the initial state is two phase, i.e., involves solid and liquid. However, recently, e.g., in the context of cooling [9,10], there emerged interest in understanding boiling near contact lines where liquid wets solid, i.e., in the initially three-phase situation. Third, in addition to cooling applications, the dewetting forced by boiling is important in the efficient scavenging of liquid away from solid or atomizing liquid such as in the case of a soap film [11] detached simultaneously from all edges on the wire frame in Fig. 1.

The experimental technique [12] for detaching liquid (soap) films from a wire is discussed in Sec. II followed by the results in Secs. III and IV. These include analysis of the transition from no detachment to nonuniform detachment and then to uniform release of soap films from wires (Sec. III A). Our understanding of the fundamental physics underlying the detachment mechanism is offered in Secs. III B and III D. A unintentionally discovered "fingering" instability, observed along the edge at the early stages of dewetting, is explored in detail in Sec. IV.

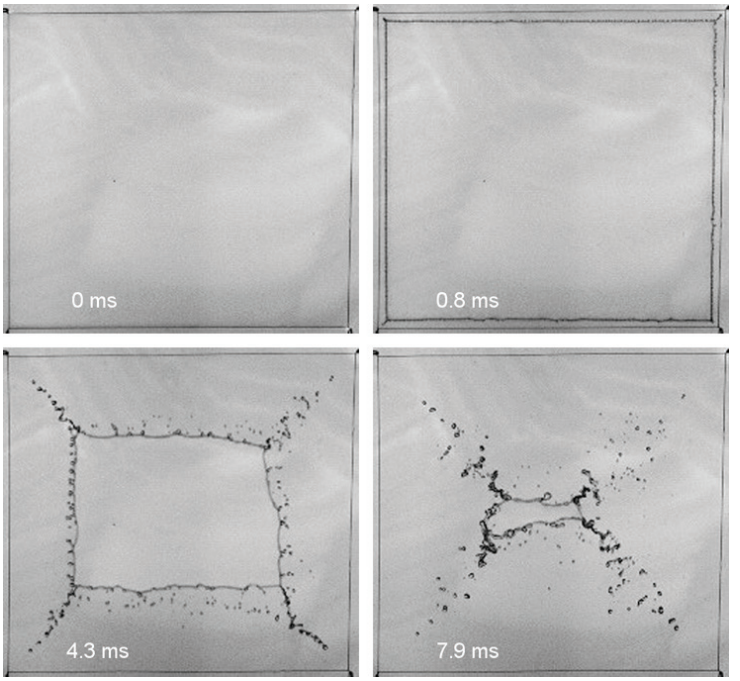

FIG. 1. Detachment and collapse of a soap film from a square (50×50 mm) frame of 40-gauge wire imaged at 8510 fps.

II. MATERIALS AND METHODS

A. Experimental setup components

Forced dewetting of the soap film shown in Fig. 1 naturally relies on Joule heating, which in turn can be made possible with the use of a continuous conducting wire that is tensioned around "sharp" corners (to minimize defects in the soap film), thus forming a rectangular frame, cf. Fig. 1 (0 ms). NiChrome (NiC) 60 bare wires (Pelican Wire Company) used in our experiments included a variety of gauge [13] sizes from 50 (wire diameter $d = 25\,\mu$m) up to 32 gauge ($d = 202\,\mu$m). Other key NiC properties include resistivity of $\varrho_w = 1.2\times10^{-6}\,\Omega\,$m, density $\rho_w = 8400\,\mathrm{kg\,m^{-3}}$, specific heat capacity $c_w = 450\,\mathrm{J\,kg^{-1}K^{-1}}$, and thermal conductivity $k_w = 13\,\mathrm{W/m\,K}$. Using a single material is intended to minimize variations in surface properties, in particular roughness—a "nuisance" variable in the boiling literature [4]. The surface properties of the wire were analyzed with a scanning electron microscope (SEM) (JEOL JSM-6390) and an optical interferometer (Bruker NPFlex with Vision64 software), cf. Fig. 2. The roughness of all the wires was found to be in the range ∼30–200 nm, i.e., on the lower end of the materials and surfaces used in traditional pool boiling experiments [14–16].

The soap film apparatus shown in Fig. 3 was constructed to accomplish two tasks: (1) using a precision stepper motor (Velmex COSMOS control software) to withdraw the soap film frame with a controlled speed in the range of 0.64–3.2 cm/s from a bath of soap solution to produce a soap film on a vertically suspended frame and (2) with a stepper motor-rotation stage (Velmex B5990TS) to rotate the frame with newly formed soap film into a horizontal position with the idea to create more uniform soap films compared to vertically oriented ones prone to gravitationally induced drainage and thus thickness variations [17].

The detachment and retraction of planar soap films was recorded using a Phantom v5.2 digital high-speed camera (Vision Research). Back lighting (i.e., transmitted light through the film) was used for clear imaging of the overall retraction and collapse of the soap films as illustrated in Fig. 1. Details of the transient shape of the film edge, which are regions of high curvature and therefore display

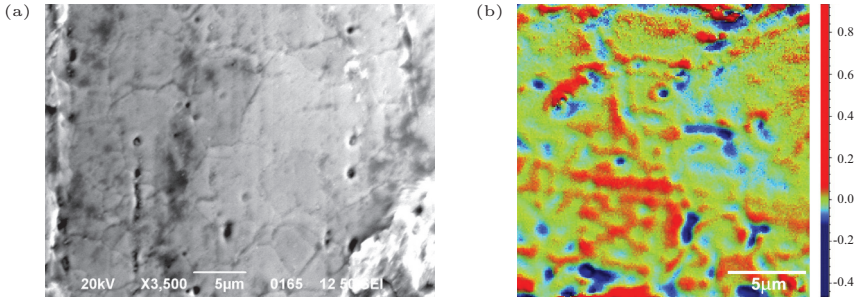

FIG. 2. Surface of NiC 60 wires of 32 gauge: (a) SEM 3500× and (b) interferometric image 20×20 μm with a color-scale bar for the roughness height given in micrometers.

high contrast if imaged using this lighting technique, were also recorded. In this approach, either a fluorescent light or a fiber optic illuminator (Dolan Jenner MI-150) was employed. In the cases, where features on the surface of the films were of interest (e.g., surface waves), a light-emitting diode (LED) lamp (LEDTronics PAR 38-12x2W-XPW-001S) and a 50R:50T plate beam splitter (Edmund Optics) were used to image light reflected from the surface thus allowing one to resolve subtle differences in curvature that are difficult to view using back lighting. Small features present along the film edge at early times were visualized with an 8-MP high-resolution digital camera (Vieworks VA-8MC-C16A0), which provides the ability to take images with exposure down to 10 ns through adjusting the time shift in triggering between the camera and the light source.

B. Circuit description

Impulsive Joule heating of the wire is accomplished through the discharge of a capacitor, cf. schematic diagram in Fig. 4. The wire forming the edges of the soap film frame acts as a conductor

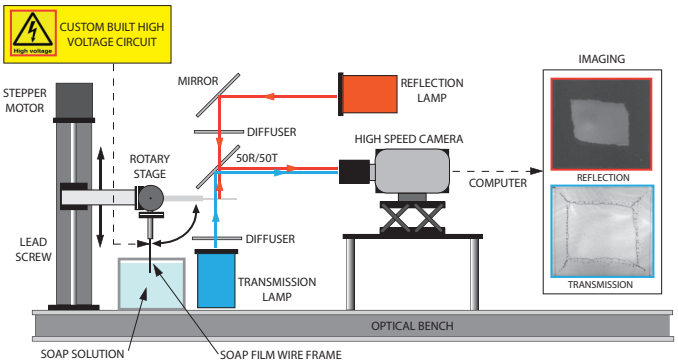

FIG. 3. Experimental setup used for the formation and detachment of planar soap films from wire frames. The stepper motor-lead screw combination (Velmex BiSlide) is used to raise and lower a bath of soap solution. The soap film wire frame is mounted on the end of an arm which is secured to the rotary stage. Formation of the soap film takes place when the arm and frame are in a vertical position, with the lowering of the bath being equivalent to the withdrawal of the frame. Once a film has been formed on the frame, it is rotated into a horizontal position and the film is illuminated using either a reflected or transmitted light source. A high-speed camera is used to capture the detachment and retraction of the film via the image reflected in the mirror. The setup is placed in an enclosure composed of extruded aluminum supports and acrylic panels and is intended to suppress the effect of air motion within the laboratory. The entire assembly is located on a vibration isolation table (Newport Corp. research series).

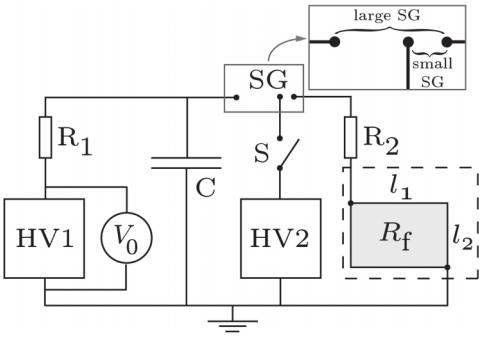

FIG. 4. Circuit used for the controlled release of a soap film formed on the wire frame with side lengths l_1 and l_2 and resistance R_f. Discharging capacitor C, charged to an initial voltage V_0, through the wire frame gives rise to Joule heating and release of the soap film. Actuation of the discharge process is accomplished by switch S and spark gap SG.

R_f consisting of two resistors in parallel, each of a total wire length $(l_1 + l_2)$. A high-voltage power supply HV1 (Spellman CZE1000R) is used to charge capacitor $C = 0.1\,\mu F$ to an initial voltage of $V_0 = 1$–$15\,kV$. The spark gap (SG), formed by two gaps as shown in Fig. 4 (a large one separates the capacitor from the soap frame and a small one is set by a second power supply HV2 to the voltage necessary to produce a spark causing breakdown of the large spark gap), is used to discharge the capacitor C through the wire frame with the switch S.

Without taking into account an inductance L of the circuit in Fig. 4, we can estimate the characteristic discharge time of the capacitor $\tau_C = R_f C \sim 1\,\mu s$. However, the presence of a nontrivial inductance, apparent in the damped oscillation of $i(t)$ shown in Fig. 5, affects this time scale. L is mainly the result of the high-voltage lead wires—16 gauge, 40 kV, silicone-insulated (UL 3239) of 2 m in length—used to carry current from the capacitor to the soap frame. To estimate the leads' inductance L, we can consider them as two parallel conductors of length l much greater than their separation distance s (the insulation thickness) and diameter d, so that the standard formula [18] $L = 0.004\,l\,[\ln(2s/d) + 1/4 - s/l]$ results in $L \sim 2.5\,\mu H$. This estimate compares favorably with the least square fit $L = 3.8\,\mu H$ between the model, formulated by applying Kirchoff's law to the

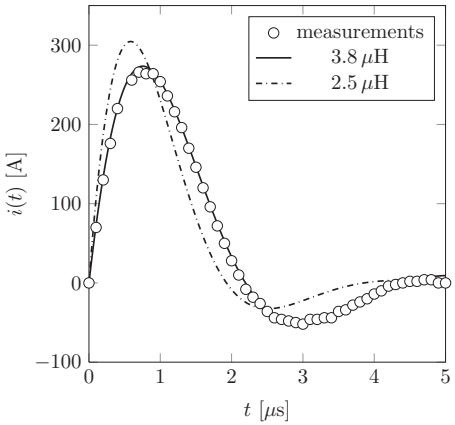

FIG. 5. Modeling results of a current $i(t)$ through the circuit using two values of inductance: $2.5\,\mu H$, estimated (dash-dotted line), and $3.8\,\mu H$, the best-fit (solid line) to the data (empty circles) measured with a Tektronix P6021 probe.

RLC circuit,

$$L\frac{di}{dt} + R\,i + \frac{1}{C}\int_0^t i(\tau)\,d\tau = 0, \tag{1}$$

and the measurements of $i(t)$, cf. Fig. 5. This value of L is the same for all experiments since all other circuit elements contribute negligible inductance, e.g., the spark gap $O(1\,\text{nH})$ [19] and the soap film frame $O(0.1\,\mu\text{H})$.

C. Soap films

Soap solutions were prepared using a mixture of deionized water (DI, 18 MΩ cm), the anionic surfactant sodium dodecyl sulfate (SDS) of 99% purity (Fisher Scientific), and glycerol (ultrapure, BP Biomedical). SDS was selected because it is well characterized and used in numerous studies of soap film formation, drainage, and retraction [20–25]. Ranges of SDS concentrations (0.5–10.0 CMC, measured in critical micelle concentration) and glycerol concentrations C_{glyc} (0–20% by weight) were tested to measure horizontal soap film lifetimes. A 1.0 CMC and 10% glycerol soap solution was chosen based on superior film lifetime [26] for the above-mentioned range of withdrawal speeds. The soap film thicknesses h_∞, measured with spectral reflectometry using a UV-VIS spectrometer (Ocean Optics USB4000-UV-VIS) and a collimated broadband light source (Dolan Jenner MI-150 or Ocean Optics LS-1), fall in the range 1–10 μm. Since all the physics we are interested in happens in the Plateau border (PB), cf. Fig. 15, which is much thicker than h_∞, we do not report the values of h_∞ as they are irrelevant for our purposes.

III. TRANSITIONS IN DEWETTING

Operationally, for any given wire diameter d and frame perimeter length $l_1 + l_2$, the control parameter is the initial voltage of the charged capacitor V_0. We will consider two fields of view: "global" such as in Fig. 1, in which we observe the detachment and collapse of the entire soap film (Sec. III A), and "detailed" in which we focus on only a small portion of the film near the wire frame (Sec. III B). Different retraction regimes associated with variations in the initial capacitor voltage V_0 will be characterized in a qualitative and quantitative fashion.

A. Global field of view observations—key regimes

From Fig. 6, we can qualitatively determine the transition from no detachment to nonuniform detachment and then to uniform detachment. From this global field of view, three basic regimes emerge that characterize the detachment and will be first discussed in terms of V_0 and then converted to the experiment-invariant variables: the discharged capacitor energy per unit wire volume and the maximum wire temperature.

1. Regime I [27]

At low voltages, the discharge of the capacitor through the wire frame *does not* lead to detachment of the film as seen in the reflected light image of Fig. 6(a) with surface waves caused by vibration of the wire frame initiated by the thermal expansion due to Joule heating. If observed for long periods of time, the waves will reflect and traverse the film several times before eventually decaying. In Fig. 7(b), regime I is denoted by the bold horizontal line corresponding to $P/P_\text{f} = 0$ for $t > 0$, where P/P_f is the fraction of the film perimeter detached from the wire as a function of time.

2. Regime II [28]

With an increase in the capacitor voltage V_0, the film is observed to detach from the wire frame but only at a select number of locations, cf. Fig. 6(b). The number of detachment locations increases with increasing the capacitor voltages shown in Fig. 6(c), where the edge has a scalloped appearance.

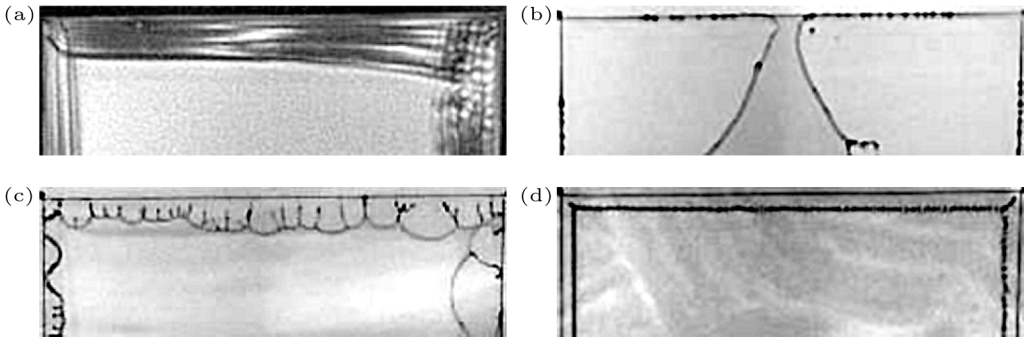

FIG. 6. Representative series of images illustrating the transition from nonuniform to uniform detachment using a global field of view for a 40-gauge wire frame 50×50 mm (only part of each image is shown): (a) 3.75 kV, regime I; (b) 4.10 kV, regime II; (c) 4.20 kV, regime II; and (d) 4.32 kV, regime III. At voltages below those needed to detach the film (a), the heating of the wire causes it to expand and vibrate resulting in surface waves (regime I). Beyond this voltage, cf. panels (b) and (c), the heating is only sufficient to initiate rupture at a finite number of sites, which are increasing with voltage (regime II). (d) With increasing voltage, the number of detachment sites is sufficiently large so that the film appears to detach *uniformly* from the wire within $\tau_{\text{fps}} = 100\,\mu$s (regime III).

This trend is presented in Fig. 7(b), where at any fixed time the value of P/P_{f} increases with voltage. Regime II corresponds to *nonuniform detachment* where the film is initially detached from the wire frame from a select number of sites. Where the film does not detach due to localized boiling, it is literally stripped from the wire by the subsequent retraction. We also observed droplets that remain attached to the wire frame, cf. Fig. 6(b), at the locations along the wire where two retracting portions of the film merge while the film edge is still attached to the wire.

3. Regime III [29]

As the capacitor voltage is further increased, a uniform detachment from the global perspective is achieved, cf. Fig. 6(d), as indicated by the bold vertical line in Fig. 7(b). The detached perimeter fraction P/P_{f} reaches a value of 1 within the time less than or equal to one frame. Unlike regime II, no stray droplets are ever observed on the wire after detachment.

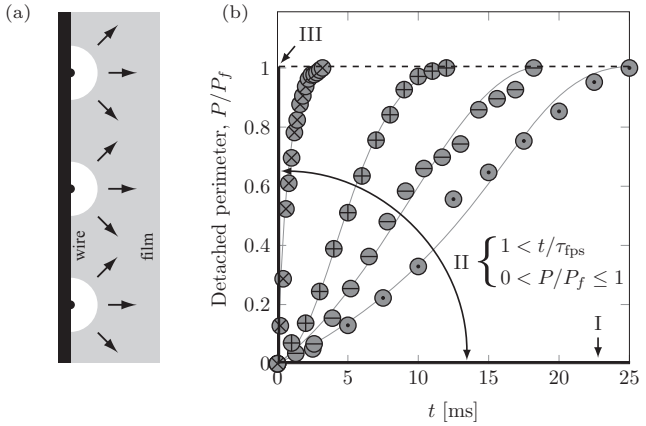

FIG. 7. (a) Detachment mechanism. (b) Perimeter detachment measurements with $\tau_{\text{fps}} = 0.1$ ms at $\odot$ 3.90, $\ominus$ 4.20, $\oplus$ 4.35, and $\otimes$ 4.50 kV. Lines through data sets are meant only to guide the eye.

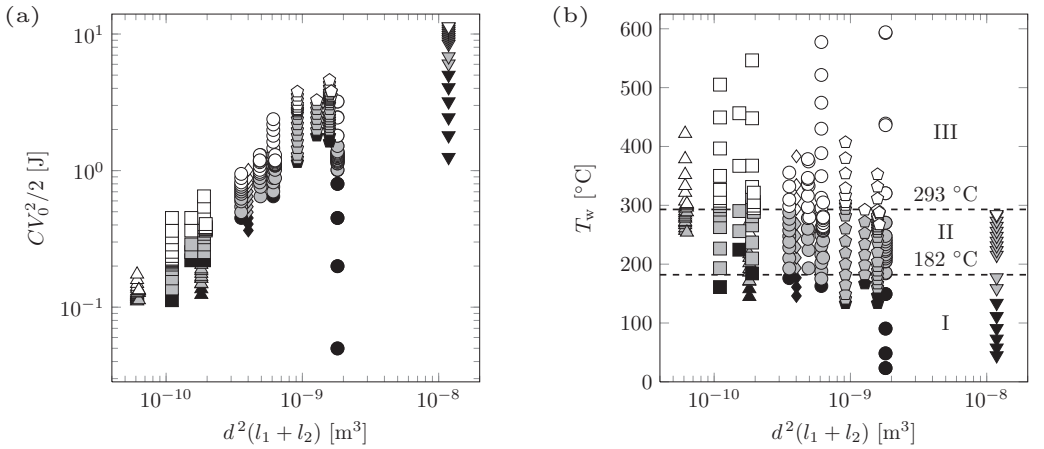

FIG. 8. Detachment measurements for a variety of wire diameters ($25 \leqslant d \leqslant 127\,\mu$m: △ 50, □ 45, ◇ 42, ◯ 40, ⌂ 36, and ▽ 32 gauge) and frame sizes ($57 \leqslant l_1 + l_2 \leqslant 290$ mm). Each column represents particular wire frame diameter and size. Moving up a column corresponds to increasing the capacitor voltage. From a global field of view, we can characterize dewetting as no detachment (I, black), nonuniform detachment (II, gray), and uniform detachment (III, open). (a) Capacitor energy versus the wire volume. (b) The transitions between the regimes occur around the same values of wire surface temperature T_w calculated using the conduction model (A3).

Uniform detachment implies that, as far as the observer can ascertain, the liquid sheet has detached from all wire points at the same instant in time. This results in an initially straight free edge of the retracting liquid sheet. However, as will be argued below, this criterion for uniform detachment depends on the field of view the observer takes and the time scale τ_{fps} over which the observation is made. Physically, impulsive Joule heating of the wire causes boiling of the liquid in contact with the wire, leading to creation of pockets of vapor that grow in size and eventually perforate the film. Let the number of nucleation sites per unit length of wire, $n = N/l$, be uniformly distributed along the wire. Given rapid growth of bubbles and the facts that the film detaches only at a nucleation site and subsequently retracts with the Taylor-Culick speed [30,31] $U_{\text{TC}} = \sqrt{2\,\gamma/\rho\,h}$ from that site, the film between two adjacent sites, cf. Fig. 7(a), will be removed from the wire in a time $\sim 1/(2\,n\,U_{\text{TC}})$; i.e., the *significant* number of nucleation sites per unit length of wire is required for uniform detachment. Thus, the appearance of uniform detachment can be expected if $\tau_{\text{fps}} \geqslant \sqrt{\rho\,d/(8\,\gamma\,n^2)}$. Here we have taken the thickness of the film h to be the diameter d of the wire, consistent with the picture that the film in the PB immediately adjacent to the wire surface has a thickness approaching that of the wire diameter. As an example, we can take $d = 25\,\mu$m (50-gauge wire), along with $\tau_{\text{fps}} = 100\,\mu$s, to arrive at the value $n_{\text{min}} \simeq 3\,000\,\text{m}^{-1}$.

Given this general understanding of the observed detachment regimes, let us first present them in terms of the experimentally controlled variables (e.g., V_0, d, etc.) in Fig. 8(a). Recognizing that the majority of the energy stored in the capacitor is initially expended in increasing the temperature of the wire via Joule heating in a near-adiabatic fashion (due to the limited quantity of heat conducted to the liquid film and negligible heat radiated to surroundings, cf. the appendix), the increase in wire surface temperature is proportional to the stored energy in the capacitor, i.e., $\Delta T_w \propto V_0^2$. Hence, we choose the vertical axis to be the energy stored in the capacitor $CV_0^2/2$ and the horizontal axis, the wire volume $d^2(l_1 + l_2)$. In terms of these variables, Fig. 8(a) suggests a linear dependence of the transition boundaries: in other words, the transitions between the regimes previously discussed occur, for various wire diameters and frame sizes, around the same values of the capacitor energy per unit wire volume. Furthermore, simple calculations show that the transition from no detachment

to nonuniform detachment occurs for values of the capacitor energy well in excess of that necessary to raise the wire surface temperature to the boiling (saturation) temperature T_{sat} of water at 1 atm.

To make a direct comparison with the literature on boiling, it will be valuable to present the above-identified three dewetting transitions in the context of the peak wire surface temperature T_w (evaluated through a transformation of capacitor voltage, cf. the appendix). For all of the wire diameters d and frame sizes $(l_1 + l_2)$ and for all of the experimental conditions (i.e., capacitor voltage), wire surface temperatures were calculated to create Fig. 8(b), in which the three detachment regimes have been denoted. To understand Fig. 8(b), we can follow a single set of data markers along a vertical line and observe the transitions discussed above. Figure 8(b) suggests that all of the wire diameters and frame sizes have approximately the same temperature associated with the transitions from no detachment to nonuniform detachment (I $\rightarrow$ II) and from nonuniform detachment to uniform detachment (II $\rightarrow$ III), as determined from the global field of view. But, the magnitudes of these transition temperatures are not quite in line with what we might expect from the simple view of boiling. For example, we might expect to observe I $\rightarrow$ II transition near $T_w \sim T_{sat} = 100\,^{\circ}\mathrm{C}$, when the onset of nucleate boiling (NB) typically occurs. But the data show an almost 80 °C increase from this temperature at the start of the nonuniform detachment regime. For the other transition, II $\rightarrow$ III, we see that the corresponding average wire temperature is near 290 °C. The magnitude of this transition temperature is also in excess of the minimum temperature required for film boiling, i.e., the Leidenfrost point [32,33], when vapor first completely blankets the heater surface.

B. Detailed field of view observations (regime II)

The detachment mechanism employed here to release soap films is reminiscent of explosive or fast transient boiling [2,6,7]. In these studies, a submerged heater—either a thin flat strip of conductive material or a small diameter wire—is provided with a pulse of electrical current from a power source. The rates of temperature increase due to such a pulse, normally in excess of 10^6 K/s, are sufficient to elevate the liquid in proximity of the heater surface well beyond the superheat temperatures necessary for nucleate boiling under steady-state conditions (cf. Fig. 11 for a representative range of values), and up to the conditions corresponding to heterogeneous or homogenous nucleation. Formation and growth of bubbles at or near the heater surface are typically of interest, and previous studies have been able to image clusters of bubbles along wires [2,6,7] and flat heaters [34] completely submerged in liquid, as well as individual nucleation sites on fabricated planar microheaters [35].

C. The mechanism of nonuniform detachment (regime II)

While the curvature of the soap solution–air interfaces in the vicinity of the wire makes visualization of individual vapor bubble formation and growth difficult, it still allows us, within regime II, to count [36] the number of detachment points N and then transform this number into nucleation sites per unit wire length $n = N/l$, i.e., a linear site (vapor bubble) density. An illustrative example of the formation and evolution of these sites is provided in Fig. 9, and the numbers n versus capacitor voltage V_0 are presented in Fig. 10(a).

We observe in Fig. 10(a) that the initial values of n are very small, but soon are followed by a rapid increase with voltage. The upper limit of these values (beyond which the uniform detachment regime III exists) is $O(1000\,\mathrm{m}^{-1})$, which is close to the estimated n_{min} value required for uniform detachment. The increase in the number of detachment sites is analogous to the rapid increase in nucleation site density with superheat temperature $\Delta T = T_w - T_{sat}$, usually expressed as a power law $n \propto \Delta T^{\alpha}$ with $\alpha \sim 5$–6, for pool boiling using factory-finished materials [4]. In fact, if we transform the site density data per unit area into the form shown in Fig. 10(b), the exponents associated with a power-law fit to these data sets are indeed in the range of 4.5–7. From Fig. 10(b), it appears that the values of site density approach a limiting value with increase in T_w, which is related to the saturation number of countable sites N due to a finite wire surface area. To demonstrate the rapid increase in nucleation sites when the transition to explosive boiling occurs, we can estimate the nucleation site

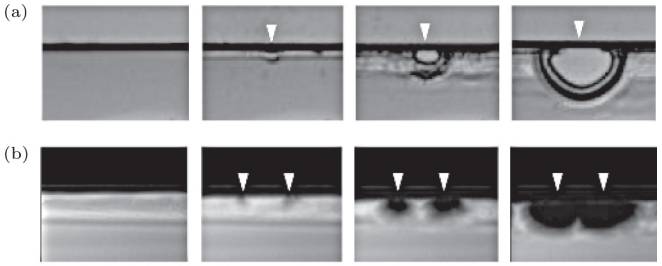

FIG. 9. Illustrative images of the growth of nucleation sites along a wire within the nonuniform detachment regime. The first image corresponds to $t \sim 0\,\mathrm{s}$, while the subsequent images represent times of 43, 216, and 430 μs. (a) A single nucleation site (indicated with the white arrow) along the 40-gauge Tungsten wire leads to perforation and retraction of the film ($T_w \sim 130^\circ$). Each image width is 1.49 mm. (b) We see two neighboring nucleation sites in the high speed movie stills showing nonuniform detachment from a 50-gauge NiC wire ($T_w \sim 192^\circ$). After perforating the film, the two receding edges eventually merge together. Each image width is 11.3 mm. The order of magnitude of the volumetric bubble growth rate is $10^2\,\mathrm{mm^3\,s^{-1}}$ in (a) and $10^5\,\mathrm{mm^3\,s^{-1}}$ in panel (b).

density for homogenous nucleation from the rate of bubble growth per unit volume [37]:

$$J = N\sqrt{\frac{3\gamma}{\pi m}}\exp\left[-\frac{16\pi\gamma^3}{3kT(\eta P_{\mathrm{sat}}(T)-P)^2}\right], \tag{2}$$

where N is the number of liquid molecules per unit volume, m the molecule mass, k the Boltzmann constant, T the liquid temperature, $P_{\mathrm{sat}}(T)$ the saturation pressure at temperature T, P the pressure of the liquid, and $\eta = \exp[(P - P_{\mathrm{sat}})/\rho RT]$ accounts for the vapor pressure inside of the bubble, where R is the gas constant for water vapor. Since we observe nucleation in the vicinity of the wire, to calculate the nucleation site density we must first integrate J from the wire surface into the PB,

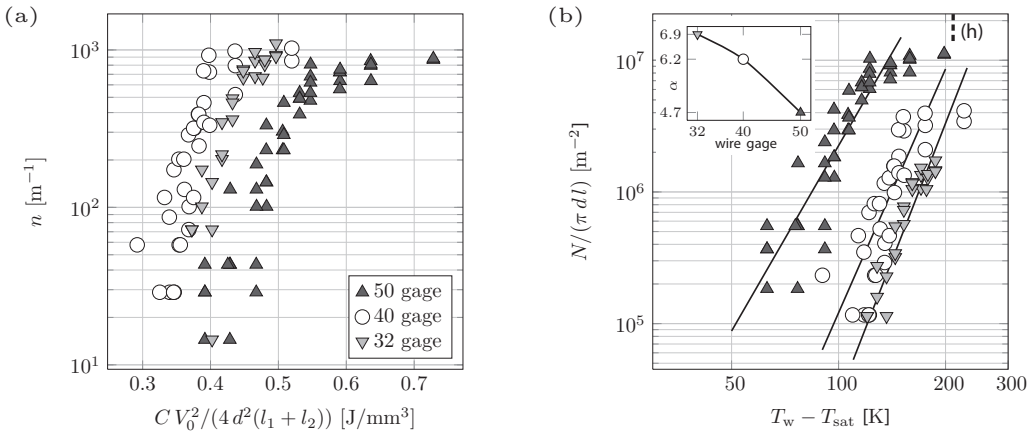

FIG. 10. Measurements of the number of nucleation sites on a long (290 mm) wire of several diameters. (a) Nucleation sites per unit length, $n = N/l$, as related to the initial capacitor energy per unit wire volume, illustrate the dramatic increase with relatively small changes in capacitor voltage. (b) Nucleation site density per unit area of the wire surface, $N/(\pi\,d\,l)$, versus wire superheat $T_w - T_{sat}$. The solid lines are power-law fits to each data set and correspond to exponents α of 4.7, 6.2, and 6.9 for the 50-, 40-, and 32-gauge wires, respectively (cf. inset). The solid, near vertical, dashed line (h) is an estimate (3) of nucleation site density for homogeneous nucleation.

cf. Fig. 15, and then over time

$$\frac{N}{\pi\, d\, l} = \int_0^t \int_{d/2}^{\delta_T} J\, dx\, dt, \tag{3}$$

where the x coordinate originates at the wire centerline and is directed toward the film, and $\delta_T = \sqrt{6\,\alpha_f\, t}$ is the thickness of a thermal boundary layer existing due to a temperature gradient in the liquid. A similar approach was employed by Iida *et al.* [34] to estimate nucleation site densities for planar heaters. As significant nucleation site densities only occur for liquid temperatures near the value corresponding to homogeneous nucleation, a very small fraction of the liquid within δ_T, which we call f, will contribute to the integral in Eq. (3). For our purposes, we can reduce the double integral to $N/(\pi\, d\, l) \simeq J(f\sqrt{\alpha_f t})t$, where we forgo the complete integral and assume, given the sensitivity of J to temperature, that sufficient temperatures exist only over a small fraction f of the thermal penetration layer developed within the PB in time t. A few degrees difference from T_w occurs over $f \sim 0.01$ and $t \sim 1\,\mu$s. With this estimate, we arrive at the solid, nearly vertical line (h) in Fig. 10(b), i.e., within a narrow range of temperatures the nucleation site density increases by orders of magnitude. Thus, our measurements of the nucleation site line density $n = N/l$, when transformed into the site density per unit area $N/(\pi\, d\, l)$, demonstrate the order of magnitude similar (on the lower end) to the site density measured in explosive boiling experiments and predicted by nucleation theory (cf. Fig. 11 of Iida *et al.* [34]).

D. The physical nature of forced dewetting

1. Transition I → II

As first noted in the global field of view analysis above (Sec. III A), despite the similarity in trend with pool boiling, there is still the question of temperatures associated with the regime II conditions. The onset of nucleate boiling for traditional pool boiling experiments in water [38], let alone a water-surfactant mixture [39], begins at small values of superheat of a few °C. We do not observe the initiation of the non-uniform detachment regime until nearly 80 °C of superheat, cf. Fig. 8(b), and surmise that there are two reasons for this. First, the delay in the onset of boiling occurs because the surface finish of the NiC wires is smoother than typical metals used for macroscale pool boiling experiments as we saw from the scanning electron microscope and interferometer images in Fig. 2. A smooth surface, with the absence of cavity sizes in typical metal heater surfaces, will delay the onset of boiling to higher values of superheat. To illustrate this trend, we can estimate the cavity diameter D_c associated with a vapor embryo in equilibrium with its surroundings [37,38] from $D_c \simeq 4\,\gamma\, T_{sat}/(\rho_v h_{fg} \Delta T)$, where ρ_v is the density of the vapor and h_{fg} the latent heat of vaporization. For water superheat of 50−100 °C we would expect $D_c \sim 10-100$ nm. These numbers are similar in magnitude to the measured 30−200 nm average surface roughness of the NiC surfaces.

Second, there is a fundamental difference between bubble growth and departure in pool boiling from our experiments. Referring back to Fig. 9, it is clear that in order to observe a site existence, the bubble must grow to a size large enough to perforate the film near the edge, i.e. to be on the order of the wire diameter d. To put it simply, if we do not see the film detach from a site, we do not observe a bubble nucleation site. In traditional pool boiling experiments, the initial stages of bubble growth are dominated by the inertia of the fluid that must be pushed away from the site. The time dependent radius for the inertia-controlled growth of a bubble is expressed as [37]

$$R(t) = \left[\frac{2}{3}\left(\frac{T_\infty - T_{sat}}{T_{sat}}\right)\frac{h_{fg}\rho_v}{\rho_l}\right]^{1/2} t, \tag{4}$$

where T_∞ is the temperature of the superheated liquid and ρ_l the density of the liquid into which the bubble grows. We can see from Eq. (4) that the rate of bubble growth increases with (increasing) superheat. Now, for our experiments, the superheat is not constant, but highly transient. In fact, the physics of the RLC circuit suggest that as the current $i(t)$ increases, the wire temperature

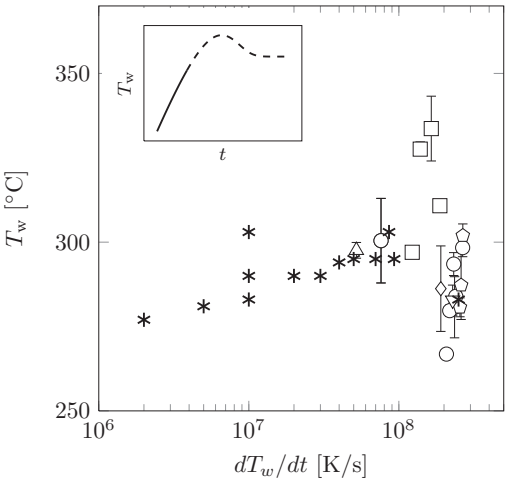

FIG. 11. The transition from nonuniform to uniform detachment occurs at temperatures similar to those observed in other explosive boiling experiments [2,6,7,34] and indicates that homogenous nucleation of the liquid is the mechanism by which bubbles form. The open (white) symbols correspond to the conditions from Fig. 8(b). Asterisk symbols correspond to values of dT_w/dt and T_w extracted from the explosive boiling literature [2,6,7,34] for experiments with water at 1 atm; no error bars are available for these data. Inset indicates qualitatively that our experiments correspond to the monotonic temperature rise regime (solid curve) before reaching the peak. We can observe that the maximum temperature growth rate in our experiments is $dT/dt \simeq 3\times10^8\,\mathrm{K\,s^{-1}}$, which corresponds to the maximum heat flux (for $d = 202\,\mu$m) of $5.7\times10^{10}\,\mathrm{W\,m^{-2}}$.

monotonically increases until it reaches a maximum. So in order for the bubble to grow to a sufficient size so as to rupture the film, under the conditions of transient power input to the wire, we must achieve a wire temperature well in excess of those typically needed for nucleate boiling from a flat plate in a pool.

2. Transition II → III

Again, it is worthwhile to comment on the differences between our experiments from traditional pool boiling. A significant departure is the rate of temperature increase in our experiments. For the experiments reported here, the uniform release of soap films from wire frames is only accomplished by a rapid release from a large number of nucleation sites along the wire, which is only possible due to an extremely fast rate of temperature increase. The estimates of wire surface temperature are based on a transient analysis and so from this approach we can also calculate the maximum value of dT_w/dt reported in Fig. 11 for the II → III transition. On the same plot are values of T_w and dT_w/dt extracted from the explosive boiling literature [2,6,7,34], which are close in magnitude to ours, thus again confirming the accuracy of our wire temperature evaluations. The reported values correspond to explosive boiling occurring due to homogeneous nucleation in the liquid (recall that under the intense pulse heating, the nucleation by fluctuation in liquid becomes the driving force for the incipience of homogeneous boiling [40]); in other words, the liquid is heated so quickly that it can be brought to the kinetic limit of superheat leading to spontaneous nucleation. The theoretical kinetic superheat for water is calculated to be in the range of 305–310 °C (depending on the nucleation density) and has been measured in explosive boiling experiments in the range of 290–310 °C, consistent with our values of wire temperature. Thus, we conclude that the II → III transition is caused by reaching an explosive boiling regime.

We can also put our experiments in the context of pool boiling on wires. A key difference between pool boiling on a flat surface and a small diameter wire is the bubble departure size: while it is on the order of capillary length in the case of pool boiling, when the wire radius (of curvature) becomes less

than the capillary length, departure of individual bubbles is suppressed. Hence, the steady boiling curve becomes monotonic compared to the hysteretic pool boiling curve on flat surfaces, i.e., there is no decrease in heat flux beyond the peak value due to suppression of nucleate boiling: instead the modes of heat transfer are natural convection, mixed film boiling, and film boiling. In explosive pool boiling on wires, the curve looks like the inset of Fig. 11: the temperature first reaches a peak and then falls to the steady-state regime, cf. Fig. 2 of Derewnicki [6]. For horizontal wires (relative to gravity), individual nucleation sites, rather than leading to bubble growth and departure, give rise to vapor patches that propagate along the wire. That is, in explosive pool boiling on wires, bubbles do not depart, while in our case they do depart due to the film detachment caused by its perforation with the expanding vapor bubbles to the state when surface tension forces are no longer capable of holding the soap film on the wire frame.

Finally, special role of surfactants in our experiments should be mentioned (besides that a surfactant is needed for the existence of a soap film). First, similar to the troubles with bubbles departure from the solid surface when boiling in low gravity conditions [41], we have boiling of a horizontally oriented film, in which the bubbles are restricted to travel only horizontally. In low gravity, in the absence of a surfactant the bubbles would coalesce to form a big primary one, which is held on to the heated surface by surface tension forces and forms a large dry patch underneath thus deteriorating high heat transfer rates due to ebullition common in Earth conditions. The use of surfactants helps to prevent bubble coalescence (similar to their role in emulsification) and thus to increase heat transfer rates [42,43], but in our case they should lead to an unwanted effect of bubbles not merging unless n is high enough. On the other hand, surfactants are known to increase the nucleation site density [44,45]. Overall, boiling performance, relative to that of pure water, is known [39] to be improved in the presence of SDS, coincidentally with optimal enhancement at or near CMC: the boiling is characterized by the formation of smaller size bubbles with increased departure frequencies and a decreased tendency to coalesce.

IV. FINGERING INSTABILITY

Although the physics of the soap film detachment that we have proposed thus far is sufficient to describe the basic nature of the transitions, features observed near the transitions between regimes appear more complex the closer we look in the neighborhood of the wire and the shorter temporal resolution is.

To highlight changes in the appearance of detachment, a series of image pairs for the detachment of soap films from a 40-gauge wire frame is provided in Fig. 12. As the capacitor voltage increases, moving from top to bottom in Fig. 12, it is obvious that there exist the regime II conditions where at early times a finite number of detachment points are present along the wire (4.20 kV, 430 μs). The finite number of detachment points lead to regions where the free edge of the film retracts in directions both away from and along the wire, eventually merging together (4.20 kV, 1100 μs). At these later times, it is evident that there are still portions of the film that remain attached to the wire as *ligaments*. The ligaments formed between merged film regions will eventually break, resulting in droplets, some of which remain attached to the wire. Such ligaments are observable as dark lines between the scallops in the global field of view images, cf. Fig. 6(c). Subtle increases in voltage, $O(100\,V)$, bring about the transition to a uniform detachment regime in which it appears that the film detaches at all points at the same time (4.32 kV, 216 μs). No ligaments are observed at these conditions and the edge of the detached liquid is approximately cylinder-like in shape, although it is apparent that some factor(s) promoted the growth of disturbances on the surface (4.32 kV, 216 μs and 430 μs).

The *most uniform* detachment in the sequence of images shown in Fig. 12 occurs for $V_0 =$ 4.32 kV, which is only 120 V larger than conditions that resulted in nonuniform detachment (i.e., $V_0 = 4.20$ kV). Beyond this value of V_0, the detachment appears uniform from a global field of view, cf. Fig. 6(d); however, a new feature—small fluid "fingers" [46]—form on the retracting edge at short times. These fingers are present near the wire for $V_0 = 4.80$–5.40 kV for $t = 86\,\mu$s. At later

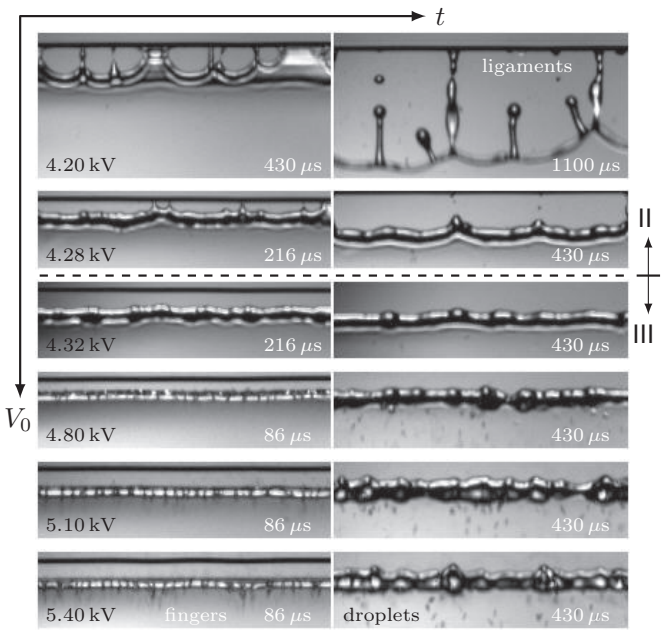

FIG. 12. Detailed field of view of the transition from nonuniform to uniform detachment (indicated by the horizontal dashed line) for a 40-gauge wire frame 50×50 mm. Images present a 4.4-mm-wide portion of the wire frame. It is evident that small changes in capacitor voltage, $O(100\,V)$, can produce noticeable differences in the appearance of the detached edge (compare 4.28 kV, 430 μs and 4.32 kV, 430 μs). Note that at voltages well beyond those needed for uniform detachment, very fine fluid fingers are observed at the receding edge. These fingers not only disrupt the shape of the edge at later times but also break up into small droplets.

times, these fingers eventually merge with the retracting edge to cause undulations on the retracting liquid rim which are not present in either the uniform or nonuniform detached edges produced at lower voltages (e.g., compare the appearance of the edge for $V_0 = 5.10$ kV at 430 μs in Fig. 12 to that of $V_0 = 4.32$ kV at 430 μs). There is also evidence that while much of the fluid mass composing these fingers merges with the edge, some is released in the form of small droplets [47] which move away from the edge, cf. Figs. 12 and 13.

The finger size and proximity to one another change with capacitor voltage (e.g., compare the differences in length, thickness, and spacing between fingers in Fig. 12 for 4.80 kV and 5.40 kV at 86 μs). The time evolution of these fingers is captured in the image sequence shown in Fig. 13 along with schematic representations of the edge detachment (drawn as cross sections). First, the edge of the film previously in contact with the wire (seen in the top of the image as the dark horizontal band) is almost completely detached and traveled a distance $\sim d$ about 10 μs after the start of the capacitor discharge. The region between the wire and the majority of the film edge appears to be traversed by remnants of a very thin liquid film and/or a large number of fine fingers (this is also sketched in the schematic). The process through which the fingers originate is considered here to occur in a series of steps.

Vapor bubbles form and expand along the wire so as to displace the PB and soap film, cf. Fig. 9, away from the wire. This is similar in behavior to the explosive vaporization of water along submerged wires subject to large heating rates, $O(10^7\,\mathrm{K/s})$ [2], except that here the vapor bubble growth leads to complete separation of the liquid (PB and soap film) from the wire. The extremely thin film of liquid that coats the wire on the side opposite to the PB is also affected by the Joule heating—being either evaporated or rapidly accelerated away from the wire after which it breaks up into drops. This is supported by the formation of a fine "mist" that appears near the wire (on the

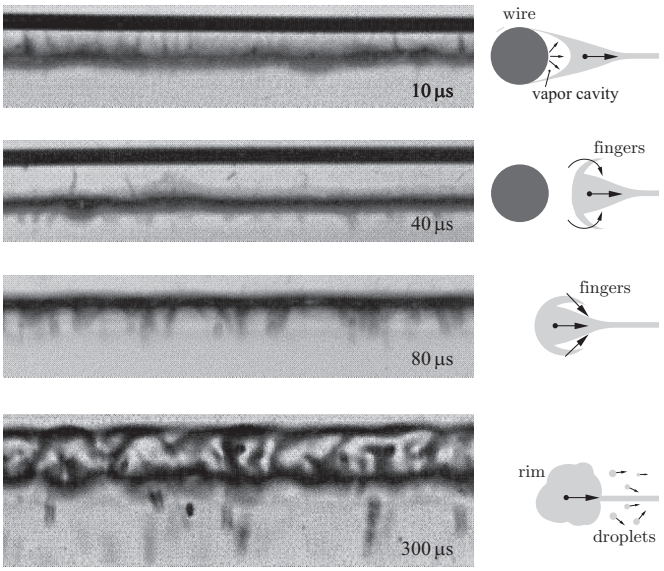

FIG. 13. Time evolution of finger formation and merger at the edge of a soap film detached from a 40-gauge wire frame ($V_0 = 5.10\,\mathrm{kV}$). Images for this sequence were acquired using a high-resolution camera and so each image is from an individual film detachment. Images present a 2.2-mm-wide portion of the wire frame, half that of Fig. 12. The finger separation distance λ_f decreases with time as fingers appear to merge and coalesce along the edge during the course of retraction. The drawings on the right are cross-sectional views (10 μs). At very early times, the soap solution in close proximity to the wire is rapidly boiled. The vapor expands pushing the film away, which leads to the formation of thinned liquid as is evident from the light area next to the wire in the image on the left. Fluid fingers, formed from the rapid vapor expansion, rotate (40 μs) and then eventually merge with the film edge (80 μs). The shape of the edge is noticeably changed after the merger into the rim (300 μs).

side opposite to the PB and retracting film) in the high-speed movies. The fingers themselves should originate from a portion of the PB liquid that has been thinned by the rapid expansion of vapor and corresponds to the lightly colored region adjacent to the wire, cf. Fig. 13 at 10 μs.

It is notable that while initially the fingers point toward the wire frame (cf. Fig. 13 at 10 μs), after $t \sim 40\,\mu$s the majority of them have rotated or folded 90–180°, which is due to the expanding vapor bubble pushing the fingers faster than the massive soap film rim retraction. Given that the fingers are about 100 μm long, this corresponds to a tip speed of the fingers near 4 m/s. The fingers are more pronounced at 80 μs and their total number has decreased. This suggests merging of fingers *along* the edge as it is retracting. Further development of this merging can be seen in Fig. 13 at 300 μs, which indicates that the separation distance between fingers λ_f increases with time until the fingers are no longer visible. Small droplets are detached from these fingers, cf. Fig. 13 at 300 μs, and at some point all fingers merge with the edge, resulting in a significant increase in the undulations on the edge surface, cf. Fig. 12 (4.32 kV, 430 μs).

The number of fingers increases with V_0 as evidenced by the finger separation distance λ_f, cf. Fig. 14. For voltages lower than those used in the plot ($V_0 < 4.6\,\mathrm{kV}$), no fingers are evident even though the detachment can still be uniform (similar to $V_0 = 4.32\,\mathrm{kV}$ in Fig. 12). The distance that most of the PB is displaced from the wire at early times (cf. the drawing in Fig. 13 at 10 μs) tends to increase with V_0 (cf. inset of Fig. 14), which is consistent with the explosive nature of the boiling process (the increase in wire heating rates with V_0).

Due to the fuzzy nature of the soap film detachment discussed in Sec. III A, it is natural that we will take the characteristic time of detachment as the time the soap film edge travels the distance

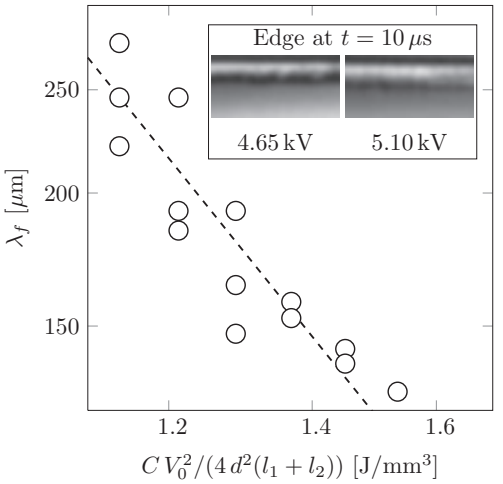

FIG. 14. Finger separation distance $\lambda_f = N_f^{-1}$ calculated from the number N_f of fingers counted per unit length of soap film edge measured at $t = 86\,\mu$s for various capacitor energies per unit wire volume within the detachment. The least square fit curve (dashed) has a slope $\beta = -2.5 \pm 0.25$. Data presented in the figure are from uniform detachment regime with a 40-gauge wire frame of 50×25 mm size. Each data point represents a measurement from a separate high-speed movie. The inset images show the size of the rapidly expanded region in close proximity to the wire for two values of V_0 that yield the formation of fingers.

on the order of the wire diameter d, i.e., $10\,\mu$s for the conditions in Fig. 13. Physically, when nucleate boiling occurs on the wire surface, it is the formation of separate vapor bubbles, which, if the nucleation density is high enough, quickly merge, form a cylindrical vapor cavity, and lead to the soap film detachment. Initially the PB is attached to the wire by surface tension and adhesion forces, but once the vapor bubble grows these forces weaken, and eventually the PB detaches from the wire as soon as the vapor bubble reaches the size of the wire diameter, cf. Fig. 13. Taking this into account, we can estimate the characteristic time of the Rayleigh-Plateau (RP) instability [48] as $t_{\rm ins} \sim \sqrt{\rho\, a^3/\gamma} \simeq 1\,\mu$s, which is shorter than the detachment time scale and hence the RP instability has time to develop. In our estimate, we took $a = d = 79\,\mu$m, the vapor density $\rho = 0.37\,$kg/m^3 at the pressure equal to 1 atm, i.e., we neglected the capillary contribution to the pressure inside the cylindrical vapor bubble since $\Delta p = 2\,\gamma/d = O(10^3\,\text{Pa}) \ll 1$ atm for the surface tension $\gamma = 38\,$mN/m of the soap film solution [49]. We should note, however, that the RP instability of the vapor cylinder may occur before it reaches the size comparable to the wire diameter. While the instability development happens on the time-growing cylindrical bubble, as an estimate of the wavelength of the RP instability we can use the standard formula $\lambda_f = 2\,\pi\, a$, which gives $\sim$150 μm, consistent with the order of magnitude measurements in Fig. 14, thus confirming viability of the RP mechanism.

However, as can be seen from Fig. 14, for higher voltages (and hence heating rates resulting in faster vapor cavity expansion rate) the instability wavelength λ_f decreases. To explain this effect, let us recall that the characteristic time of instability $t_{\rm ins}$ is the result of competition between inertia of the fluid cylinder of radius a and the surface tension force. From this formula, it follows that the time t required to reach the radius a, at which a RP instability develops, scales as $a \sim t^{2/3}$. Hence, the instability wavelength $\lambda = 2\,\pi\, a \sim t^{2/3}$. The time t it takes for the vapor cavity to grow to this critical size a becomes shorter with the increase of the capacitor energy (Joule heating) [cf. Eq. (A3)] and hence λ_f should decrease with increasing V_0, which is qualitatively seen in Fig. 14. The actual exponent β in the dependence $\lambda_f \sim (C\,V_0^2)^\beta$ (and hence the vapor cavity size growth) will depend not only on the wire temperature growth rate responsible for the heat supplied for the vapor bubble

growth, but as per Eq. (A3) also on the circuit inductance L, which sets the current $i(t)$ growth rate, cf. Eq. (1) and Fig. 5.

V. CONCLUSIONS

We have presented an experimental study of forced dewetting liquid sheets on wires. Impulsive Joule heating of metal wire frames enables the formation of nearly straight edges of soap films, which is achieved when the liquid adjacent to the wire is heated rapidly to a temperature sufficient to cause spontaneous nucleation and "explosive boiling." Observations of the detachment of the film edges indicate that this process is substantially different from that of explosive boiling on wires completely submerged into the bulk liquid: namely, in the latter case bubbles do not depart but rather propagate along the wire, while in our case they do depart due to the film detachment caused by its perforation with the expanding vapor bubbles. Moreover, the film detachment happens before the temperature reaches a peak of the explosive boiling curve for fully submerged wires; cf. inset of Fig. 11. Transitions between the key identified dewetting regimes—no detachment, nonuniform detachment, and uniform detachment of a film—differentiated by boiling transitions in the film Plateau borders prove to occur, for various wire diameters and frame sizes, around the same values of the capacitor energy per unite wire volume corresponding to approximately the same wire temperatures. The formation of liquid "fingers" on the film edge during its early stage of evolution, for voltages in excess of those required for uniform detachment, was discovered via detailed imaging of the detachment process. The origin of these fingers is attributed to the RP instability.

While in the present work we focused on the film dewetting stage, the subsequent retraction dynamics may have its own interesting physics, especially in view of its difference from the classical approach of rupturing a soap film at a single point, e.g., via a passage of an alcohol-covered ball [50] or a spark [51]. Namely, in the case of a point rupture a circular hole with a small radius and hence initial large curvature is formed so that its edge (rim) stretches as it retracts, whereas a straight film edge does not have a longitudinal curvature and thus no axial stretching should be present. Later stages of the film retraction could also be interesting due to the development of along-the-edge instabilities [52], cusp formation [53], and eventual film atomization [22]—processes deserving a separate study.

ACKNOWLEDGMENTS

This work was partially supported by the National Science Foundation (NSF) CAREER Award No. 1054267 and the Natural Sciences and Engineering Research Council of Canada (NSERC) Grant No. 6186. The authors would like to thank Jason Martin, Jamie Booth, and Gilbran Alvarez for their help at the preliminary stages of setting up the soap film detachment experiments. H.C.M. is also grateful to Greg Dahlen (UCSB) for kindly lending the Tektronix P6021 needed for high-resolution imaging and Verne Parmenter (UCSB, retired) for the help with the development of the experimental setup. R.K. also acknowledges many stimulating conversations with Andrei Zelnikov on various theoretical aspects of the phenomena presented here.

APPENDIX: WIRE TEMPERATURE

The film dewetting happens over a finite time (due to the fluid inertia) and, since the heating is fast and transient, over a range of temperatures rather than at a concrete onset temperature. Other sources of the wire temperature uncertainty come from its increase at boiling incipience with heating rate in explosive boiling (cf. Fig. 9 of Glod *et al.* [2]) and nonuniform heating of the wire due to the skin effect to be discussed below. Therefore, while the wire temperature in some boiling experiments is measured directly with a calibrated resistance technique (in which the resistance of the frame is monitored electrically and related to the wire temperature through the known temperature coefficient of resistance), in order to get a better insight into the phenomena we instead determine

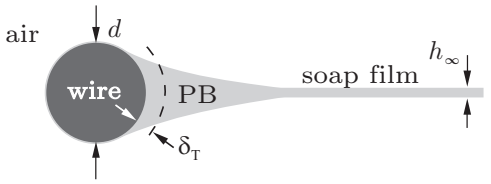

FIG. 15. The geometry used in model (A3): the PB spanning from the wire to uniform soap film of thickness h_∞, through which heat is conducted from the wire.

the wire temperature from an appropriate thermodynamic model. The model predictions are verified independently by comparing them with measurements in the literature, cf. Fig. 11. This allows us to highlight the heat transfer processes occurring once the wire is heated impulsively and to challenge the common viewpoint that the fast heating is adiabatic.

Let us first estimate the contributions of convection and radiation to the heat transfer processes. Recall that the soap film frame is oriented horizontally. If the wire temperature is set instantaneously to T_w, then the heat will propagate in a fluid within a thermal boundary layer of thickness $\delta_\mathrm{T} = \sqrt{6\,\alpha_\mathrm{f}\,t}$ with thermal diffusivity $\alpha_\mathrm{f} = 3.0{\times}10^{-7}\,\mathrm{m}^2/\mathrm{s}$ (note that $\alpha_\mathrm{f} = k_\mathrm{f}/\rho_\mathrm{f}\,c_\mathrm{f}^p$), i.e., it is the mass $\sim\delta_\mathrm{T}\,d\,\rho_\mathrm{f}$, which is being accelerated due to the Archimedes force $\sim\delta_\mathrm{T}\,d\,\Delta\rho_\mathrm{f}\,g$, where $\Delta\rho_\mathrm{f} = \rho_\mathrm{f}\,\beta_T\,(T_\mathrm{w} - T_\mathrm{f})$ with the coefficient of thermal expansion $\beta_T = 3.4{\times}10^{-3}\,\mathrm{K}^{-1}$. This gives the characteristic time of convection in air

$$t_\mathrm{conv} \simeq \alpha_\mathrm{f}^{1/3}\,[g\,\beta_T\,(T_\mathrm{w} - T_\mathrm{f})]^{-2/3} = O(1)\,\mathrm{s}, \tag{A1}$$

i.e., much slower than the time scales of our experiments; note that the air viscosity ν_f sets the same time scale because $\nu_\mathrm{f} = O(\alpha_\mathrm{f})$. Next, the radiation and conduction fluxes will become comparable at time t when

$$\frac{\epsilon\,\sigma}{h}\,\frac{T_\mathrm{w}^4 - T_\mathrm{f}^4}{T_\mathrm{w} - T_\mathrm{f}} \simeq 1, \tag{A2}$$

where σ is the Stefan-Boltzmann constant, ϵ the emissivity of the wire surface, and $h = k_\mathrm{f}/\delta_\mathrm{T}$ the conduction coefficient. In the case of water, this happens when $t = O(10^4)\,\mathrm{s}$ and for air $t = O(0.1)\,\mathrm{s}$, i.e., again on much longer time scales compared to our experiments, so that we can safely neglect radiation effects as well.

With these considerations, the energy balance for the wire involves Joule heating $P_\mathrm{J} = i^2(t)\,R_\mathrm{f}$ and conduction only:

$$C_\mathrm{w}^p\,\frac{dT}{dt} = P_\mathrm{J} - h\,A_s(T - T_\mathrm{f}), \tag{A3}$$

where $A_s = \pi\,d\,l$ is the wire surface area, $C_\mathrm{w}^p = \rho_\mathrm{w}\,A_c\,l\,c_\mathrm{w}^p$ wire heat capacity, $A_c = \pi\,d^2/2$ the wire cross section, and T_f the temperature of the ambient fluid.

Due to the transient nature of the current of frequency $\omega/(2\pi)$ on the order of 1 MHz, we find the depth of the skin layer $\delta \sim \sqrt{2\,\varrho_\mathrm{w}/(\omega\,\mu)} \simeq 10\,\mu\mathrm{m}$, where ϱ_w is the wire material resistivity and μ the magnetic permeability of the wire material. Hence, especially for larger wires, the heat is generated at the wire surface. This, however, brings up the question of temperature variation inside the wire—which can, nevertheless, be neglected for our purposes [54]. Indeed, thermal diffusivity of water is much smaller than that of wire $\alpha_\mathrm{f} \ll \alpha_\mathrm{w}$, where $\alpha_\mathrm{f} = 1.6{\times}10^{-7}\,\mathrm{m}^2/\mathrm{s}$ vs $\alpha_\mathrm{w} = 3.4{\times}10^{-6}\,\mathrm{m}^2/\mathrm{s}$, so that from the heat conduction $T_t = \alpha\,\nabla^2 T$ we conclude $t_\mathrm{w}/t_\mathrm{f} = \alpha_\mathrm{f}/\alpha_\mathrm{w} \ll 1$, which means that the temperature in the wire equilibrates much faster. While in the case of air $t_\mathrm{w}/t_\mathrm{f} = \alpha_\mathrm{f}/\alpha_\mathrm{w} \gg 1$, for the same time t the affected volumes in metal $\sim\sqrt{\alpha_\mathrm{w}\,t}$ and air $\sim\sqrt{\alpha_\mathrm{f}\,t}$ have

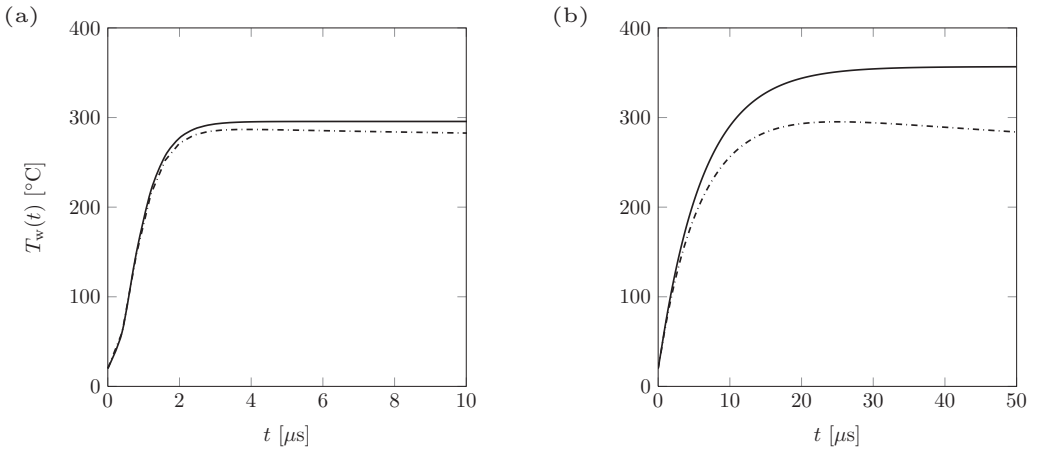

FIG. 16. Comparison of the difference in transient wire surface temperatures $T_w(t)$ between the adiabatic model (solid lines) and conduction model (dashed lines) for wire frames of size 26×76 mm: (left) 40 gauge and (right) 50 gauge.

the ratio of heat capacities:

$$\frac{\rho_w}{\rho_f}\frac{c_w^p}{c_f^p}\sqrt{\frac{\alpha_w}{\alpha_f}} \gg 1, \tag{A4}$$

where the specific heat capacity of air $c_f^p = 1\,\mathrm{kJ\,kg^{-1}K^{-1}}$ vs that of wire $c_w^p = 0.450\,\mathrm{kJ\,kg^{-1}K^{-1}}$. From an analogous argument, we assess the importance of conduction based on the time required for the wire $C_w^p = \frac{\pi}{4}\rho_w\, c_w^p\, d^2$ and fluid $C_f^p = \rho_f\, c_f^p\, \pi\, d\, \delta_T$ heat capacities per unit wire length to become of the same order:

$$t_{\mathrm{cond}} \simeq \left(\frac{\rho_w}{\rho_f}\right)^2\left(\frac{c_w^p}{c_f^p}\right)^2\frac{d^2}{96\alpha_f}. \tag{A5}$$

Using water as a conducting fluid, we get $t_{\mathrm{cond}} = 33\,\mu$s for $d = 25\,\mu$m and $t_{\mathrm{cond}} = 2.1$ ms for $d = 202\,\mu$m wire, i.e., conduction becomes non-negligible in the case of small diameter wires. While adiabatic model neglecting conduction gives reasonable estimates of T_w, for small diameter wires the correction due to conduction brings T_w in agreement with the values for large diameter wires; neglecting conduction into the liquid within the PB leads to an overestimation of the wire temperature, which is more pronounced for smaller diameter wires and is on the order of ∼20 °C, cf. Fig. 16. Our evaluation of the wire surface temperature $T_w(t)$ is based on Joule heating of the wire material and conduction of heat into the part of PB of volume $V_{\mathrm{PB},\delta}$ (cf. Fig. 15), namely a region near the wire surface that penetrates into the PB by a depth [8,55] $\delta_T(t) \sim 2\sqrt{\alpha_f t}$, which is for water $O(1\text{–}10)\,\mu$m, i.e., much smaller than d for $t = 1\text{–}10\,\mu$s. Typical results for $T_w(t)$ obtained by integrating (A3) are presented in Fig. 16 and compared to the adiabatic model when $h = 0$.

[1] R. R. Allen, J. D. Mayer, and W. R. Knight, Thermodynamics and hydrodynamics of thermal ink jets, Hewlett-Packard J. **36**, 21 (1985).

[2] S. Glod, D. Poulikakos, Z. Zhao, and G. Yadigaroglu, An investigation of microscale explosive vaporization of water on an ultrathin Pt wire, Int. J. Heat Mass Transfer **45**, 367 (2002).

[3] T. G. Karayiannisa and M. M. Mahmoud, Flow boiling in microchannels: Fundamentals and applications, Appl. Thermal Eng. **115**, 1372 (2017).
[4] J. H. Lienhard, *A Heat Transfer Book* (Prentice-Hall, Englewood Cliffs, NJ, 1981).
[5] N. Bakhru and J. H. Lienhard, Boiling from small cylinders, Int. J. Heat Mass Transfer **15**, 2011 (1971).
[6] K. P. Derewnicki, Vapour bubble formation during fast transient boiling on a wire, Int. J. Heat Mass Transfer **26**, 1408 (1983).
[7] K. P. Derewnicki, Experimental studies of heat transfer and vapour formation in fast transient boiling, Int. J. Heat Mass Transfer **28**, 2085 (1985).
[8] J. Nardin, C. Poulain, and J. Duplat, Incipience of boiling on a wire, Int. J. Heat Mass Transfer **55**, 6881 (2012).
[9] A. J. Robinson, Heat transfer near the contact line during boiling in microgravity, Microgr. Sci. Tech. **19**, 139 (2007).
[10] S.-Y. Park and Y. Nam, Single-sided digital microfluidic (sdmf) devices for effective coolant delivery and enhanced two-phase cooling, Micromachines **8**, 3 (2017).
[11] The film is produced by withdrawal from a soap solution at speed of 2.5 cm/s and released at $V_0 = 5100$ V.
[12] Forget bubbles: Free-flying soap sheets created for the first time, MIT Technol. Rev. (October 15, 2010).
[13] E. A. Avallone, T. Baumeister, and A. Sadegh, *Mark's Standard Handbook for Mechanical Engineers* (McGraw-Hill, New York, 2006).
[14] I. L. Pioro, W. Rohsenow, and S. S. Doerffer, Nucleate pool-boiling heat transfer. II: Assessment of prediction methods, Int. J. Heat Mass Transfer **47**, 5045 (2004).
[15] R. J. Benjamin and A. R. Balakrishnan, Nucleation site density in pool boiling of saturated pure liquids: Effect of surface microroughness and surface and liquid physical properties, Exp. Thermal Fluid Sci. **15**, 32 (1997).
[16] E.g., emery paper finish gives the following roughness values: copper, 70–1400 nm; aluminum, 520–3600 nm; brass, 500 nm; nickel, 50 nm; and stainless steel, 200–500 nm.
[17] K. J. Mysels, K. Shinoda, and S. Frankel, *Soap Films: Studies of Their Thinning* (Pergamon Press, New York, 1959).
[18] F. W. Grover, *Inductance Calculations: Working Formulas and Tables* (Dover, New York, 1962).
[19] P. Persephonis, K. Vlachos, C. Georgiades, and J. Parthenios, The inductance of the discharge in a spark gap, J. Appl. Phys. **71**, 4755 (1992).
[20] K. J. Mysels and M. C. Cox, An experimental test of Frankel's law of film thickness, J. Colloid Sci. **17**, 136 (1962).
[21] J. Lyklema, P. C. Scholten, and K. J. Mysels, Flow in thin liquid films, J. Phys. Chem. **69**, 116 (1965).
[22] W. R. McEntee and K. J. Mysels, The bursting of soap films. I. An experimental study, J. Phys. Chem. **73**, 3018 (1969).
[23] L. J. Evers, S. Y. Shulepov, and G. Frens, Rupture of thin liquid films from Newtonian and viscoelastic liquids, Faraday Discuss. **104**, 335 (1996).
[24] P. D. T. Huibers and D. O. Shah, Multispectral determination of soap film thickness, Langmuir **13**, 5995 (1997).
[25] S. Berg, E. A. Adelizzi, and S. M. Troian, Experimental study of entrainment and drainage flows in microscale soap films, Langmuir **21**, 3867 (2005).
[26] As is also consistent with the choices in the literature [22,25].
[27] See Supplemental Material at http://link.aps.org/supplemental/10.1103/PhysRevFluids.2.094003 for regime I.
[28] See Supplemental Material at http://link.aps.org/supplemental/10.1103/PhysRevFluids.2.094003 for regime II.
[29] See Supplemental Material at http://link.aps.org/supplemental/10.1103/PhysRevFluids.2.094003 for regime III.
[30] G. I. Taylor, The dynamics of thin sheets of fluid. III. Distintegration of fluid sheets, Proc. R. Soc. London, Ser. A **253**, 313 (1959).
[31] F. E. C. Culick, Comments on a ruptured soap film, J. Appl. Phys. **31**, 1128 (1960).
[32] F. M. White, *Heat Transfer* (Addison-Wesley, Reading, MA, 1984).

[33] J. D. Bernardin and I. Mudawar, The Leidenfrost point: Experimental study and assessment of existing models, Trans. ASME **121**, 894 (1999).
[34] Y. Iida, K. Okuyama, and K. Sakurai, Boiling nucleation on a very small film heater subjected to extremely rapid heating, Int. J. Heat Mass Transfer **37**, 2771 (1994).
[35] K. M. Balss, C. T. Avedisian, R. E. Cavicchi, and M. J. Tarlov, Nanosecond imaging of microboiling behavior on pulsed-heated Au films modified with hydrophilic and hydrophobic self-assembled monolayers, Langmuir **21**, 10459 (2005).
[36] We limited our experiments to three wire diameters and one frame size for these experiments.
[37] V. P. Carey, *Liquid-Vapor Phase-Change Phenomena* (Taylor & Francis, Philadelphia, 2008).
[38] V. K. Dhir, Boiling heat transfer, Annu. Rev. Fluid Mech. **30**, 365 (1998).
[39] V. M. Wasekar and R. M. Manglik, Pool boiling heat transfer in aqueous solutions of an anionic surfactant, Trans. ASME **122**, 708 (2000).
[40] J. Li, G. P. Peterson, and P. Cheng, Mechanical nonequilibrium considerations in homogeneous bubble nucleation for unsteady-state boiling, Int. J. Heat Mass Transfer **48**, 3081 (2005).
[41] M. Q. Raza, N. Kumar, and R. Raj, Surfactants for bubble removal against buoyancy, Sci. Rep. **6**, 19113 (2016).
[42] J. Clunie, J. Goodman, and P. Symons, Solvation forces in soap films, Nature (London) **216**, 1203 (1968).
[43] N. Duerr-Auster, R. Gunde, R. Mäder, and E. J. Windhab, Binary coalescence of gas bubbles in the presence of a non-ionic surfactant, J. Colloid Interface Sci. **333**, 579 (2009).
[44] G. Hetsroni, A. Mosyak, E. Pogrebnyak, I. Sher, and Z. Segal, Bubble growth in saturated pool boiling in water and surfactant solution, Int. J. Multiphase Flow **32**, 159 (2006).
[45] H. J. Cho, J. P. Mizerak, and E. N. Wang, Turning bubbles on and off during boiling using charged surfactants, Nat. Commun. **6**, 8599 (2015).
[46] It should be clarified that these new "fingers" are *not* the same fingers reported by McEntee and Mysels [22]. The fingers that we observed originate along soap film edges released from wire frames, exist for only a very short period of time, and are estimated to be considerably smaller in size than the features reported by McEntee and Mysels.
[47] See Supplemental Material at http://link.aps.org/supplemental/10.1103/PhysRevFluids.2.094003 for a movie illustrating the formation of droplets.
[48] P. G. Drazin and W. H. Reid, *Hydrodynamic Stability* (Cambridge University Press, Cambridge, UK, 2004).
[49] Since we are away from the critical point for water (373.95 °C and 217.7 atm).
[50] Lord Rayleigh, Some applications of photography, Nature (London) **44**, 249 (1891).
[51] W. E. Ranz, Some experiments on the dynamics of liquid films, J. Appl. Phys. **30**, 1950 (1959).
[52] R. Krechetnikov, Stability of liquid sheet edges, Phys. Fluids **22**, 092101 (2010).
[53] J. M. Gordillo, H. Lhuissier, and E. Villermaux, On the cusps bordering liquid sheets, J. Fluid Mech. **754**, R1 (2014).
[54] But it may affect the accuracy of direct measurements with a Wheatstone bridge.
[55] The penetration depth in this case differs slightly (the constant changing from $\sqrt{6} \to 2$) because $\delta_T \ll d$ and the PB does not completely surround the wire.